# In-depth study of degradation in scalable wide bandgap perovskite cells

OPEN ACCESS
IOP Publishing | Songshan Lake Materials Laboratory

MATERIALS FUTURES

Mater. Futures 4 (2025) 045101 (8pp) https://doi.org/10.1088/2752-5724/ae01c1

# In-depth study of degradation in scalable wide bandgap perovskite cells

**Jonathan Parion[1,2,3,4,*], Baptiste Jacquet[1,3,4], Dawar Ali[5,6], Raju Pusapati[1,3,4], Amit Kumar Harit[1,3,4], Aurora Rizzo[6], Yinghuan Kuang[1,3,4], Filip Duerinckx[1,3,4], Hariharsudan Sivaramakrishnan Radhakrishnan[1,3,4], Tom Aernouts[1,3,4], Anurag Krishna[1,3,4], Jef Poortmans[1,3,4,7], Johan Lauwaert[2] and Bart Vermang[1,3,4,*]**

[1] Hasselt University, Wetenschapspark 1, 3590 Diepenbeek, Belgium
[2] Department of Electronics and Information Systems, Ghent University, Technology Park 126, 9052 Zwijnaarde, Belgium
[3] imec division IMOMEC,Thorpark 8320, 3600 Genk, Belgium
[4] EnergyVille, Thorpark 8320, 3600 Genk, Belgium
[5] University of Salento, Via Lecce-Monteroni, 73047 Monteroni di Lecce LE, Italy
[6] CNR NANOTEC—Istituto di Nanotecnologia, c/o Campus Ecotekne, Via Monteroni, 73100 Lecce, Italy
[7] KU Leuven, Department of Electrical Engineering, Kasteelpark Arenberg 10, 3001 Leuven, Belgium

E-mail: jonathan.parion@imec.be and bart.vermang@uhasselt.be

Received 28 July 2025, revised 25 August 2025
Accepted for publication 1 September 2025
Published 16 September 2025

**Abstract**

Perovskite solar cells with a wide bandgap (WBG) perovskite absorber of 1.68 eV are fabricated and their performance evolution under accelerated stressing conditions are compared with 1.61 eV reference devices. The cells are processed entirely with scalable deposition methods, to guarantee their relevance for industrial application. Different stress tests, following the International Summit on Organic Photovoltaic Stability (ISOS) protocols, are performed, namely prolonged exposure to light (ISOS-L1), heat (ISOS-D2) and a combination of these (ISOS-L2). First, the ISOS-L1 test highlights the excellent stability of the chosen WBG composition, with minimal degradation after 60 h. Secondly, the ISOS-D2 test led to a more significant degradation of the WBG cells, with only 80% efficiency retained after 95 h. The main cause of degradation was found to be interface-related, specifically the formation of a charge transport barrier at the perovskite/electron transport layer interface, while the perovskite absorption properties remained unaffected by the stress test. Finally, the ISOS-L2 test led to an even faster degradation, with only 80% efficiency retained after 35 h. There, the perovskite absorber itself was found to be significantly degraded due to the combined action of light and heat. Altogether, this study highlights the main degradation pathways in WBG perovskite cells while showing the importance of diversified and combined stresses in evaluating their stability.

* Authors to whom any correspondence should be addressed.

Supplementary material for this article is available online

Keywords: perovskite solar cells, wide bandgap perovskite, perovskite degradation, ISOS protocols, halide segregation, S-shape

## 1. Introduction

Wide bandgap (WBG) perovskites have lately attracted increased attention, mainly due to their promising optoelectronic properties making them suitable candidates to be integrated as top cell absorber in tandem solar cells (TSCs). Particularly good candidates for such application are the hybrid-organic lead halide perovskites with a bandgap around 1.7 eV, since they can be combined with silicon cells to theoretically reach the highest possible efficiency in TSCs [1]. In spite of this, these WBG perovskites typically face poor stability under light and at elevated temperatures. This is because, to widen the bandgap of the perovskite, bromide ($Br^-$) is mixed with iodide ($I^-$) to occupy the halide site of the perovskite crystal. When submitted to light, these species segregate into Br-rich and I-rich domains, leading to the formation of regions with a higher and lower bandgap, respectively. As a consequence, photo-generated carriers are driven towards the low bandgap regions, where their recombination is facilitated, therefore causing significant device performance loss [2]. To mitigate this phenomenon, various techniques have been explored, among which additive, composition and interface engineering, as well as precise crystallization control [3–7]. However, while these approaches typically enable good stability of the perovskite film under continuous illumination, there are only few reports of the stability of fully functional devices under different stressing conditions. Moreover, the vast majority of works where stability of devices is reported focus on showcasing the performance evolution rather than on understanding the root cause of the degradation. Finally, most of the devices reported in the literature were manufactured using lab-scale, non-scalable techniques such as spin-coating, which limit their relevance for industrial application. Therefore, an in-depth analysis of the degradation mechanisms of WBG perovskite devices, made by scalable deposition techniques, under different stressing conditions is required.

In this work, perovskite solar cells with a bandgap of 1.68 eV are fabricated and their stability is compared with stable 1.61 eV reference cells. These devices are made using scalable techniques, and submitted to three standardized accelerated stress tests derived from the International Summit on Organic Photovoltaic Stability (ISOS) protocols, namely ISOS-L1, ISOS-D2 and ISOS-L2 [8]. To study and understand the degradation mechanisms occurring in these devices, an electrical characterization toolbox, combining current–voltage (*I–V*), photoluminescence (PL) and capacity–frequency (*C–f*) measurements is used.

In a first section, the WBG and reference devices are compared in terms of stability under the three different stress tests mentioned above. One sample of each type was selected for each of the tests to be shown in this work, but these tests were repeated over a larger amount of samples and the same trends were consistently observed. As anticipated, the reference devices show a significantly higher stability in all three tests. Interestingly, not all three tests lead to the same degradation rate. Therefore, in a second section, an in-depth analysis is performed on samples submitted to the two stress tests leading to the fastest degradation, i.e. the ISOS-D2 and ISOS-L2 tests. This analysis reveals the distinct degradation pathways that are occurring during these tests, highlighting the importance of using diversified and combined stress tests when analyzing perovskite device stability.

## 2. Experimental details

### 2.1. Device fabrication

Perovskite solar cells with a semi-transparent p–i–n device architecture were fabricated with the following stack: glass/ITO/hole transport layer (HTL)/perovskite/electron transport layer (ETL)/ITO, using scalable methods. Each 9 $cm^2$ sample is composed of 12 small pixel cells with an area of 0.125 $cm^2$. Two perovskite absorbers, both deposited by blade-coating, were used: 'reference' 1.61 eV with $Cs_{0.2}FA_{0.8}Pb(I_{0.94}Br_{0.06})_3$ composition and 'wide-bandgap' 1.68 eV with $Cs_{0.15}(MA_{0.2}FA_{0.8})_{0.85}Pb(I_{0.8}Br_{0.2})_3$ composition. For the HTL, a 15 nm layer of $NiO_x$ was deposited by DC sputtering. For the ETL, a stack of LiF/$C_{60}$/LiF with thickness 0.8/15/0.8 nm was deposited on top of the perovskite by thermal evaporation. The reference 1.61 eV perovskite layer was previously demonstrated to be very stable under ISOS-D2 accelerated testing [9], therefore motivating its choice as a reference for this study. The IV curve and main figure of merits for both a champion reference and WBG cell are given in supplementary information figure S1.

### 2.2. Device characterization

Current–voltage (*I–V*) measurements were performed in a $N_2$ environment, using an Abet Sun 3000 solar simulator. The light intensity was calibrated to 100 mW $cm^{-2}$ using Fraunhofer ISE's WPVS reference solar cell (Type: RS-ID-4). A Keithley 2602A source meter was used to record the *I–V* characteristic in both reverse and the forward directions, with a scan speed of 0.13 V $s^{-1}$. PL measurements were performed in ambient air, at 45% relative humidity and a temperature of 22 °C, using a Picoquant Fluotime 300 lifetime and steady state spectrometer. The emitter is composed of a 20 mW laser source of wavelength $\lambda = 532$ nm, pulsed at 40 MHz. Capacitance–frequency (*C–f*) measurements were carried out in a $N_2$ environment and in the dark, using the Fluxim PAIOS

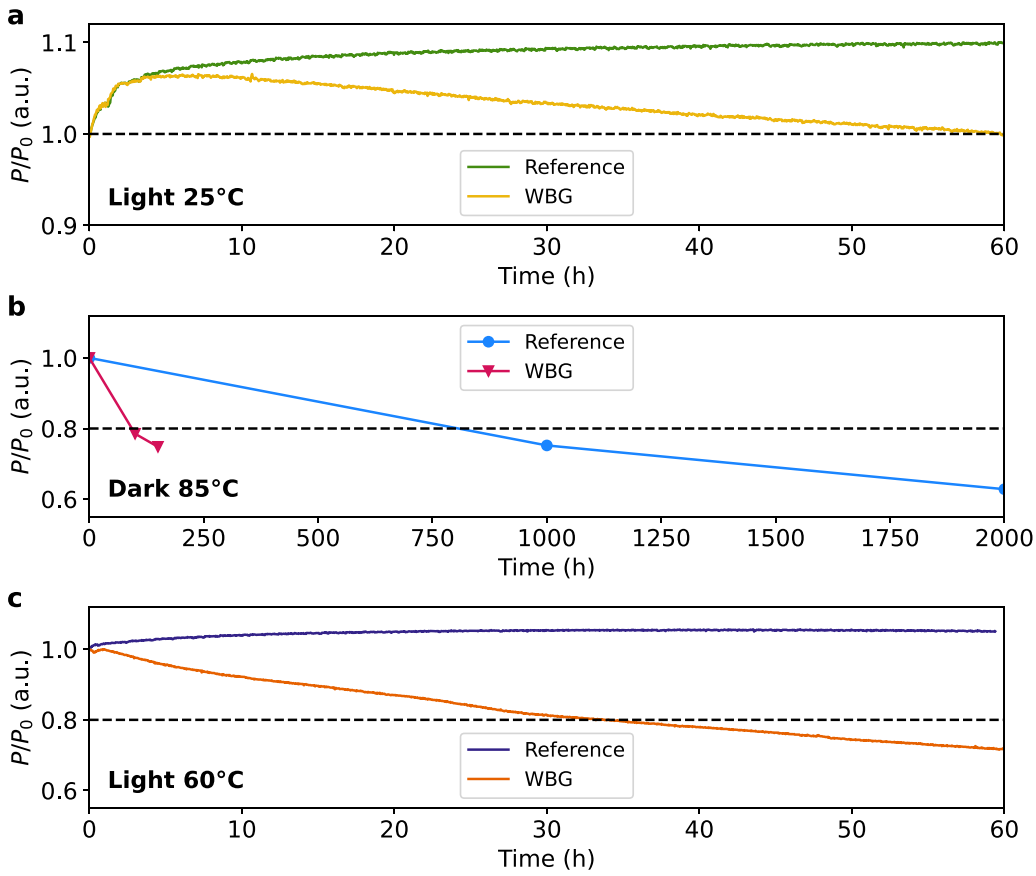


**Figure 1.** Performance evolution of the reference vs wide bandgap (WBG) samples under different stressing conditions: (a) ISOS-L1: maximum power point tracking (MPPT) under 1 Sun illumination at 25 °C, (b) ISOS-D2: dark storage at 85 °C and (c) ISOS-L2: MPPT under 1 Sun illumination at 60 °C. All tests were performed in a $N_2$ environment.

system. During measurement, the sample is kept at 0 V DC bias and a small AC signal of 30 mV is applied.

## 3. Performance evolution under different stressing conditions

A common step in evaluating the stability of WBG perovskites is usually to test the stability of the emission peak of the bare absorber under continuous PL illumination at 25 °C in $N_2$. The red-shift of the PL emission peak with time is attributed to the formation of I-rich domains in the absorber owing to light-induced halide phase segregation [3]. A logical conclusion emerging from these studies is that light-induced phase segregation is a major degradation pathway in WBG perovskites.

Since this work focuses on the stability of full devices, a WBG perovskite solar cell was subjected to light-soaking using the ISOS-L1 protocol, and the device maximum power point (MPP) was tracked at 1 Sun illumination, at a temperature of 25 °C and in a $N_2$ environment. The performance evolution of the WBG cell, compared to reference, is shown in figure 1(a). Both the reference and WBG cell exhibit a strong improvement in performance during the initial period (<5 h) of light-soaking. After this, while the reference cell displayed a saturating and stable behavior with an overall improvement of 10%, the WBG cell showed a constant degradation over the remainder of the test until 60 h, albeit not catastrophic. This shows that the perovskite composition has a clear impact on the stability behavior under exposure to light, and that only light-soaking might not be sufficient to cause a significant and fast degradation of the WBG perovskite absorber.

The WBG and reference samples were also submitted to two other accelerated ageing tests, namely the ISOS-D2 protocol, where the performance evolution after dark storage at 85 °C and in $N_2$ is followed (figure 1(b)) as well as the ISOS-L2 protocol, where the MPP at 1 Sun illumination, 60 °C and in a $N_2$ is tracked continuously (figure 1(c)). In both cases, the performance of the WBG perovskite cells shows a much faster degradation rate, with a time to 80% performance ($t_{80}$) reached after only 95 h and 35 h respectively. In the case of the ISOS-D2 stress test, performance loss could also be observed for the reference cell, though after a significantly longer time. In the next section, further insight is gathered on the degradation of WBG perovskite submitted to the ISOS-D2 and ISOS-L2 protocols. Specifically, the aim is to understand how the cells degrade in both cases, and whether a different origin can be identified for each case.

## 4. In-depth analysis of the device degradation

### *4.1. ISOS-D2 stress test*

During the ISOS-D2 stress test, the reference and WBG samples were periodically characterized using *IV*, PL and *C–f* measurements. In figures 2(a) and (b), showing the *IV* curves at different stages of degradation, a similar behavior is observed for both the reference and the WBG cells, although on a much shorter timescale for the latter. Initially, only a reduction in open-circuit voltage ($V_{oc}$) is observed. With long durations of dark storage, an 'S-shape' starts to appear close to the $V_{oc}$ point, heavily impacting the fill-factor (FF). The short-circuit current ($J_{sc}$) varies little with time, suggesting that the absorber layer is not much affected by the stress test. Finally, the hysteresis of the *IV* curve seems to increase with degradation in the WBG cell but not in the reference cell. This last observation could indicate a possible link between degradation in the WBG cell and mobile ionic charges, which is further discussed below.

The formation of an S-shape characteristic in the IV curves has previously been reported in the literature for perovskite solar cells, and each time attributed to the formation of a barrier at one of the perovskite/transport layer (TL) interfaces [10–12]. This barrier can typically either be an extraction barrier, caused by a highly resistive TL, or an injection barrier, formed in the presence of a band alignment mismatch at the interface. As explained by W. Tress and O. Inganäs in [10], performing light-dependent *IV* measurements enables to distinguish between these two cases. This was done for the WBG sample, as shown in figure S2 of the supplementary information. At lower light intensities, the FF increases and the S-shape disappears, which is a clear sign of an extraction barrier. Such a barrier typically appears in the presence of low-mobility TLs. In these circumstances, a potential drop occurs over the highly resistive TL, which then behaves similarly to a dielectric layer in a capacitor. This has the effect of reducing the built-in electrical field in the perovskite, affecting the photo-generated current at high light intensities. Eventually, this leads to a lower FF and to a slight reduction in $J_{sc}$. One plausible origin for this extraction barrier would be the deterioration of the ETL after the thermal stress test. The ETL stack, and specifically the $C_{60}$ layer, is prone to degradation under these conditions, which could eventually result in an increased layer resistivity [13, 14]. This conclusion was moreover confirmed in a recent work, that used TCAD simulations to uncover the origin of the degradation in devices using a similar architecture [15]. The perovskite morphology and its roughness are known to exacerbate this degradation issue, possibly explaining the difference in stability between the reference and the WBG samples.

To delve further into the origin of the degradation and understand whether the same degradation mechanism is occurring in the reference and WBG cells, PL measurements are performed on the pristine vs degraded devices, as shown in figures 2(c) and (d). Neither the reference nor the WBG sample exhibits PL shift over time, indicating that no phase segregation is taking place in these cells during the dark stress test. The PL intensity, however, changes with time, which usually corresponds to a change in quasi–Fermi level splitting [16, 17]. This result is partly in line with the observations from the *IV* measurements in figures 2(a) and (b), in the sense that there is indeed a reduction in $V_{oc}$ occurring between the first and second measurement. However, between the second and third measurement, a difference in PL intensity is observed, whereas no difference in $V_{oc}$ is recorded for both cell types. This suggests that the PL intensity can also depend on other factors, the most significant being interface recombination properties, as already reported in [17–19]. This would corroborate the hypothesis formulated earlier that an interface issue would be the main cause of degradation in these samples, beyond the initial loss in $V_{oc}$.

Finally, to go one step further in understanding the degradation of these cells, *C–f* measurements are performed. As previously discussed in [20, 21], this type of measurement provides more information on the perovskite absorber itself, enabling the extraction of its geometric capacitance as well as the analysis of its mobile ions dynamics. The measurement for both the reference and WBG sample is represented in figures 2(e) and (f), respectively. First, the geometric capacitance ($C_{geo}$) is extracted in the medium frequency region ($10^2 - 10^5$ Hz), and is computed as

$$C_{geo} = \frac{\varepsilon_0 \varepsilon_{pero}}{t_{pero}} \tag{1}$$

$\varepsilon_{pero}$ being the dielectric permittivity of the perovskite layer and $t_{pero}$ its thickness. Since $C_{geo}$ stays constant with time and because it is an intrinsic parameter to that layer, a logical deduction is that the perovskite layer properties remained unaffected by the stress test, which is in line with earlier interpretations. This is also further motivated by x-ray diffraction (XRD) measurements performed on these samples (supplementary information figure S3) which do not exhibit any sign of phase segregation or decomposition of the active perovskite phase into inactive amorphous phases.

In the low-frequency region, clear differences are observed between the two samples. For the reference sample (figure 2(e)), the low-frequency response stays constant with degradation time. On the other hand, for the WBG sample (figure 2(f)), the transition frequency at which the capacitance starts increasing is shifted to the higher frequencies with degradation. As discussed by Messmer *et al* in [21] regarding *C–f* measurements performed on similar samples, this indicates that the ionic diffusivity increases with degradation in the WBG sample. Moreover, since the low-frequency capacitance is also higher in absolute value than for the reference case, a higher density of mobile ionic charges in the WBG cell is also very likely. This is an important observation, which was not possible to deduce from the previous measurements, and which is moreover independent of the phase segregation mechanism, shown not to occur in these cells.

Overall, these different results enable to conclude on the nature of degradation occurring in the dark and under

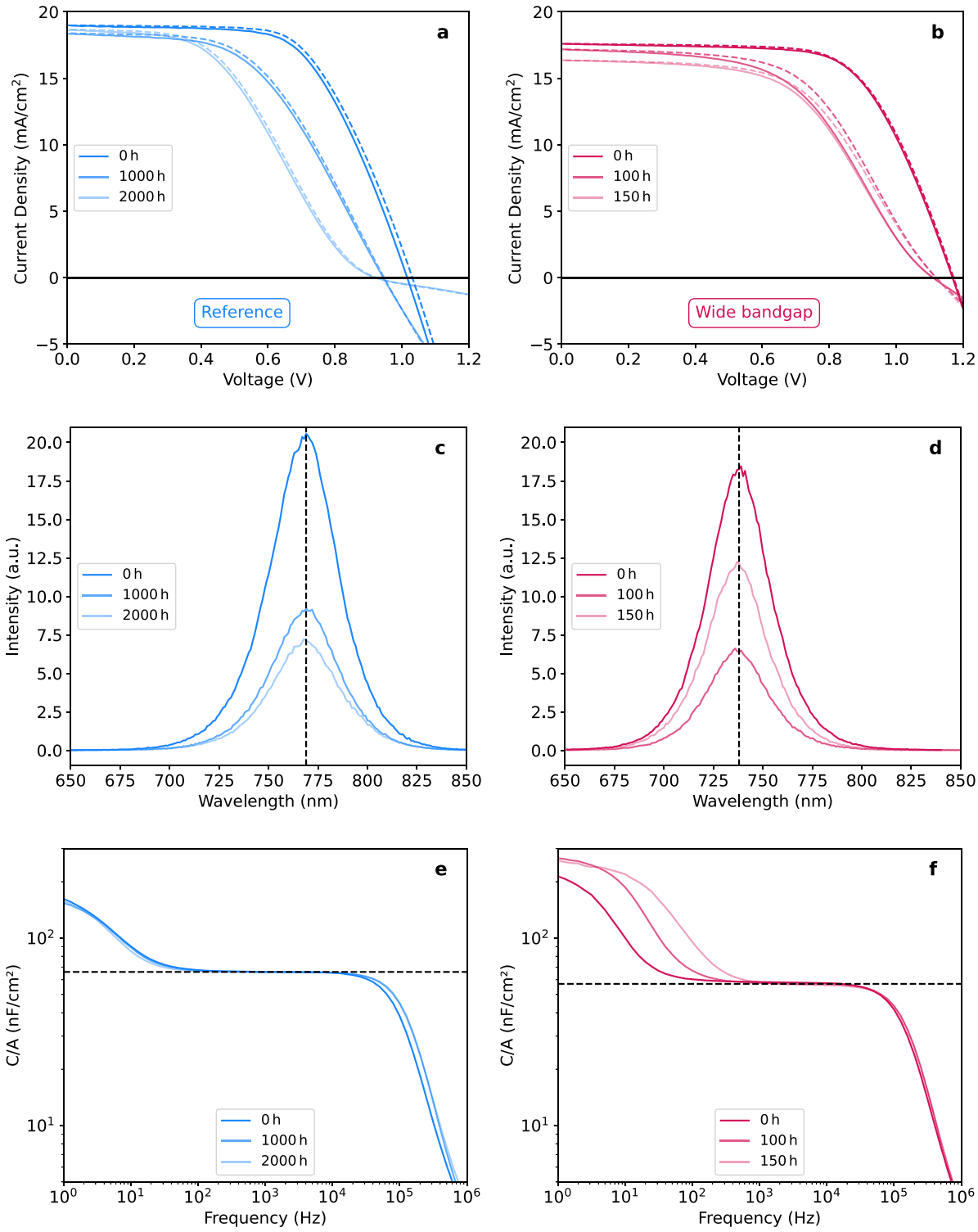


**Figure 2.** Evolution of the *IV* curve with time for (a) the reference cell and (b) the wide bandgap cell stored in the dark, at 85 °C and in $N_2$ (ISOS-D2 test). The solid and dashed curves represent respectively the forward and reverse *IV* scans. Steady-state photoluminescence measurements of the (c) reference and (d) wide bandgap sample at different degradation times. The dashed line highlights in both cases the position of the PL peak, not shifting with degradation time. Capacitance–frequency measurements of (f) the reference and (g) the wide bandgap samples at different degradation times. The dashed line highlights in both cases the position of the geometric capacitance $C_{geo}$.

85 °C thermal stress. Under these conditions, the perovskite layer absorption properties remain unchanged, for both the reference and WBG samples. The main cause for degradation of these samples is found to be interface-related, likely at the perovskite/ETL interface. The *IV* characteristic shows the formation of an S-shape, pointing towards the existence of a charge extraction barrier at that interface. For the WBG samples, a higher density of ions is moreover observed,

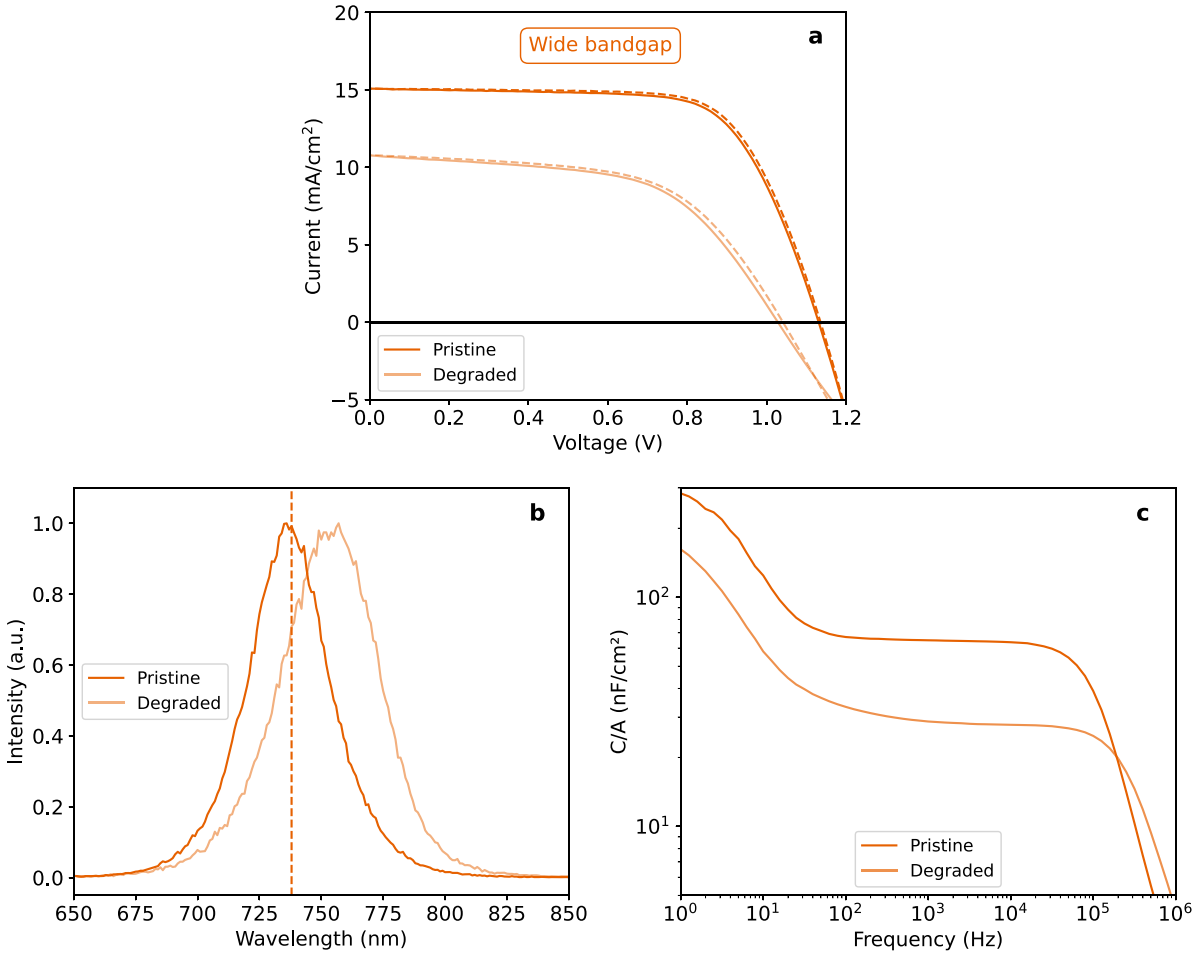


**Figure 3.** (a) Evolution of the wide bandgap cell *IV* curve before and after being tracked at its maximum power point under 1 Sun illumination, at 60 °C and in $N_2$ (ISOS-L2 test) for 60 h. The solid and dashed curves represent respectively the forward and reverse *IV* scans. (b) Normalized steady-state photoluminescence measurements of the wide bandgap sample before and after the ISOS-L2 stress test. The dashed line highlights the position of the initial PL peak, shifting with degradation time. (c) Capacitance–frequency measurements of the wide bandgap samples at before and after the ISOS-L2 stress test.

with increasing diffusivity with stressing time. This might potentially be related to the interface issue, as the redistribution of these ions has the ability to modify the interface properties, by changing its extraction properties [22] or by chemically reacting with the TL material [23, 24]. This would however require further investigation to be confirmed. In the next section, the same characterization methodology is applied to study the degradation of these cells under light and heat.

### *4.2. ISOS-L2 stress test*

For this stress test, as previously mentioned, the MPP of the sample was tracked under light, at 1 Sun intensity, and at a constant temperature of 60 °C. Since very little performance loss is observed for the reference sample (figure 1(c)), the analysis focuses on the WBG cell that is at the core of this study. The *IV* plots in figure 3(a) for the WBG sample before and after the ISOS-L2 test show that in addition to a reduction in $V_{oc}$ and FF (as was in the case of ISOS-D2), there is also a strong reduction in $J_{sc}$. The most plausible explanation for the strong $J_{sc}$ loss is a degradation of the absorber itself, and hence a lower ability to generate electrical charges. This current loss is furthermore confirmed by external quantum efficiency measurements realized on a similar sample submitted to the same protocol (supplementary info, figure S4).

The steady-state PL spectrum of the cells before and after degradation shows a clear red shift after degradation, as depicted in figure 3(b). Again, this is likely a sign of the formation of I-rich domains in the absorber. Moreover, since these measurements are not performed directly after the ISOS-L2 stress test, the formation of these domains seems to be permanent. It indicates that the absorber layer has irreversibly degraded, contrary to what was observed for the stress test in the dark.

This observation is confirmed by the *C–f* measurements, as shown in figure 3(c). There, the flat region at medium frequencies ($10^2$–$10^5$ Hz), where $C_{geo}$ is extracted, is very clearly impacted by the ISOS-L2 stress test, showing a strong reduction for the degraded sample. Based on equation (1), this indicates that the dielectric permittivity of the perovskite, $\varepsilon_{pero}$, is significantly affected by degradation. Following the Drude model of semiconductors, changes in the chemical composition of a material directly affect its bandstructure, its density of

states and therefore also its dielectric constant [25]. Moreover, $\varepsilon_{pero}$ is also directly related to the intrinsic polarisability of the perovskite layer [26]. Therefore, if the chemical composition of the perovskite is altered, e.g. by the appearance of different phases, the polarisability can also be modified. More specifically in this case, new phases with lower crystallinity and a higher lattice disorder, as confirmed by XRD measurements (supplementary information figure S5), could lead to a reduced response of the perovskite to the displacement field which then results in a lower $\varepsilon_{pero}$. This shows that a reduction in $C_{geo}$ is a good way of confirming the modification of the perovskite layer. The low-frequency response of the device, on the other hand, seems to be much less affected by the degradation, as observed when normalizing the capacitance response by $C_{geo}$ (supplementary info, figure S6). Following our previous analysis, this indicates that there is little variation in the ionic diffusivity of the layer, which is an interesting observation since ions have often been reported to be at the root of degradation in perovskite-based devices.

Overall, this analysis clearly shows that the degradation of perovskite devices submitted to light and high-temperature conditions, following the ISOS-L2 protocol, is very different from the one occurring in the dark and at elevated temperatures. Under light and heat, the degradation is most likely absorber-related, with a significantly reduced ability to generate a photo-current and clear phase segregation. Moreover, when comparing the MPP tracking under light and at elevated temperatures to the results under light but at lower temperatures from figure 1, it appears very clearly that the combined action of light and heat is needed in order to observe fast degradation of the WBG perovskite absorber when embedded in a full cell stack. This is another important finding, since previous studies tend to mainly link illumination with phase segregation as being the principal degradation mechanism in WBG perovskites.

## 5. Conclusion

In this work, the stability of WBG perovskite solar cell under different stressing conditions was thoroughly investigated. First, MPP tracking of these devices at room temperature and 1 Sun irradiance was found to cause relatively minimal performance loss, against the common knowledge that light is the main degradation factor in WBG perovskites. Then, the impact of dark storage at 85 °C temperature was studied, and found to not cause degradation of the perovskite absorber. Instead, the fast performance degradation observed for the WBG devices in these circumstances was attributed to the deterioration of the perovskite/ETL interface, possibly due its weak thermomechanical stability. Finally, the combined impact of the exposure to 1 Sun light intensity and to an elevated temperature of 60 °C on the WBG cell was investigated, and found to cause significant degradation of the perovskite absorber. This important finding emphasizes the role of heat on the phase segregation process and on the degradation of WBG perovskites under operational conditions, which was overlooked in many previous studies. As next steps, non-destructive characterization such as GIWAXS, LBIC, and EBIC can be applied to further probe the structural and chemical state of the device. Altogether, this study shows the importance of carrying out a set of diversified accelerated ageing protocols and a thorough study beyond the sole analysis of performance evolution to unravel the key degradation mechanisms in WBG perovskite solar cells.

## 6. Future perspectives

In this work, similarly to others before, the systematic lower stability of WBG perovskite solar cells compared to similar narrow bandgap perovskite devices was demonstrated. Furthermore, it emerged that different degradation modes are observed in different stressing conditions, emphasizing that 'perovskite stability' may not be an absolute concept. For this reason, several steps are yet to be undertaken before this material becomes suitable for industrial-scale deployment. First, a more detailed understanding of the nanoscale-level degradation in different stressing conditions is required. This goes in parallel with efforts to improve the stability of the WGB perovskite, not only at material but also at cell and module level. Secondly, these devices should be tested in a wider range of stressing conditions, potentially leading to the discovery of new degradation modes. Outdoor field deployment is central among these tests, as it mimics the real-life operation of devices and should highlight which accelerated tests are the most representative to reproduce these conditions. Finally, when moving towards the commercialization of this technology, clear industrial standards for stability should be set and coupled with adapted and standardized accelerated stress tests.

## Data availability statement

The data supporting these findings is included as part of the supplementary information.

## Acknowledgments

The authors gratefully thank Daniely Santos (UHasselt and imo-imomec) for her support in obtaining the XRD measurements. J P acknowledges the financial support by the Fonds Wetenschappelijke onderzoek (FWO) with Grant Number 1S01525N. A K, Y K, and T A acknowledge the financial support by the European Union's Horizon Europe research and innovation programme under grant agreement No. 101147311 of the LAPERITIVO project and grant agreement No. 101120397 of the Approach project.

## Conflicts of interests

The authors declare no conflicts of interests.

## Authors contribution

Conceptualization: J. Pa., A. K.; data curation: J. Pa., B. J.; formal analysis: J. Pa., B. J.; funding acquisition: J. Pa., F. D., H. S. R., J. Po., J. L., B. V.; investigation: J. Pa., B. J., D. A., R. P., A. K. H.; methodology: J. Pa., B. J., A. K.; project administration: J. Pa., B. J., A. K.; resources: H. S. R., T. A., A. K., J. Po., J. L., B. V.; software: J. Pa., B. J.; supervision: A. R., Y. K., F. D., H. S. R., T. A., A. K., J. Po., J. L., B. V.; validation: A. K.; visualization: J. Pa., B. J., A. K.; writing—original draft: J. Pa.; writing—review & editing: all co-authors.

## ORCID iDs

Jonathan Parion 0000-0002-8695-917X
Raju Pusapati 0009-0004-2913-5694
Amit Kumar Harit 0000-0002-5125-6626
Aurora Rizzo 0000-0002-4570-7777
Yinghuan Kuang 0000-0002-1564-842X
Filip Duerinckx 0000-0003-2570-7371
Hariharsudan Sivaramakrishnan Radhakrishnan 0000-0003-1963-273X
Tom Aernouts 0000-0002-3004-6080
Anurag Krishna 0000-0001-7255-7412
Jef Poortmans 0000-0003-2077-2545
Johan Lauwaert 0000-0002-0757-2509
Bart Vermang 0000-0003-2669-2087

## References

[1] Bremner S P, Levy M Y and Honsberg C B 2008 Analysis of tandem solar cell efficiencies under AM1.5G spectrum using a rapid flux calculation method *Prog. Photovolt., Res. Appl.* **16** 225–33
[2] Nie T, Jia L, Feng J, Yang S, Ding J, Liu S and Fang Z 2025 Advances in single-halogen wide-bandgap perovskite solar cells *Adv. Funct. Mater.* **35** 2416264
[3] Fang Z, Nie T, Liu S and Ding J 2024 Overcoming phase segregation in wide-bandgap perovskites: from progress to perspective *Adv. Funct. Mater.* **34** 2404402
[4] Wang S, Li M-H, Jiang Y and Hu J-S 2023 Instability of solution-processed perovskite films: origin and mitigation strategies *Mater. Futures* **2** 012102
[5] Li M-H, Gong X, Wang S, Li L, Fu J, Wu J, Tan Z and Hu J-S 2024 Facile hydrogen-bonding assisted crystallization modulation for large-area high-quality CsPbI2Br films and efficient solar cells *Angew. Chem., Int. Ed.* **63** e202318591
[6] Li M-H *et al* 2023 Hydrogen-bonding-facilitated dimethylammonium extraction for stable and efficient $CsPbI_3$ solar cells with environmentally benign processing *Joule* **7** 2595–608
[7] Li M-H, Ma X, Fu J, Wang S, Wu J, Long R and Hu J-S 2024 Molecularly tailored perovskite/poly(3-hexylthiophene) interfaces for high-performance solar cells *Energy Environ. Sci.* **17** 5513–20
[8] Khenkin M V *et al* 2020 Consensus statement for stability assessment and reporting for perovskite photovoltaics based on ISOS procedures *Nat. Energy* **5** 35–49
[9] Tutundzic M *et al* 2024 Toward efficient and fully scalable sputtered $NiO_x$-based inverted perovskite solar modules via co-ordinated modification strategies *Sol. RRL* **8** 2300862
[10] Tress W and Inganäs O 2013 Simple experimental test to distinguish extraction and injection barriers at the electrodes of (organic) solar cells with S-shaped current-voltage characteristics *Sol. Energy Mater. Sol. Cells* **117** 599–603
[11] Chiang S-E, Wu J-R, Cheng H-M, Hsu C-L, Shen J-L, Yuan C-T and Chang S H 2019 Origins of the S-shape characteristic in J-V curve of inverted-type perovskite solar cells *Nanotechnology* **31** 115403
[12] Saive R 2019 S-shaped current-voltage characteristics in solar cells: a review *IEEE J. Photovolt.* **9** 1477–84
[13] De Bastiani M *et al* 2022 Mechanical Reliability of fullerene/tin oxide interfaces in monolithic perovskite/silicon tandem cells *ACS Energy Lett.* **7** 827–33
[14] Erdil U *et al* 2024 Delamination of perovskite solar cells in thermal cycling and outdoor tests *Energy Technol.* **13** 2401280
[15] Parion J *et al* 2025 A novel way of analyzing perovskite outdoor degradation: the S-Voc *EES Sol.* (https://doi.org/10.1039/D5EL00079C)
[16] Stolterfoht M *et al* 2018 Visualization and suppression of interfacial recombination for high-efficiency large-area pin perovskite solar cells *Nat. Energy* **3** 847–54
[17] Stolterfoht M, Le Corre V M, Feuerstein M, Caprioglio P, Koster L J A and Neher D 2019 Voltage-dependent photoluminescence and how it correlates with the fill factor and open-circuit voltage in perovskite solar cells *ACS Energy Lett.* **4** 2887–92
[18] Stoddard R J, Eickemeyer F T, Katahara J K and Hillhouse H W 2017 Correlation between photoluminescence and carrier transport and a simple in situ passivation method for high-bandgap hybrid perovskites *J. Phys. Chem. Lett.* **8** 3289–98
[19] Campanari V *et al* 2022 Reevaluation of photoluminescence intensity as an indicator of efficiency in perovskite solar cells *Sol. RRL* **6** 2200049
[20] Parion J, Ramesh S, Subramaniam S, Vrielinck H, Duerinckx F, Radhakrishnan H S, Poortmans J, Lauwaert J and Vermang B 2024 Multifaceted characterization methodology for understanding nonidealities in perovskite solar cells: a passivation case study *Sol. RRL* **8** 2400529
[21] Messmer C, Parion J, Meza C V, Ramesh S, Bivour M, Heydarian M, Schön J, Radhakrishnan H S, Schubert M C and Glunz S W 2024 Understanding ion-related performance losses in perovskite-based solar cells by capacitance measurements and simulation *Sol. RRL* **8** 2400630
[22] Neukom M T *et al* 2019 Consistent device simulation model describing perovskite solar cells in steady-state, transient and frequency domain *ACS Appl. Mater. Interfaces* **11** 23320–8
[23] Hussain T, Fatima K, Anjum A, Abbas T A, Ahmad I, Fakharuddin A and Sultan M 2022 Experimental evidence of ion migration in aged inorganic perovskite solar cells using non-destructive RBS depth profiling *Mater. Adv.* **3** 7846–53
[24] Miah M H, Rahman M B, Alam M, N-E-Islam M A, Shahinuzzaman M, Rahman M R, Ullah M H and Khandaker M U 2025 Key degradation mechanisms of perovskite solar cells and strategies for enhanced stability: issues and prospects *RSC Adv.* **15** 628–54
[25] Kittel C 2005 *Introduction to Solid State Physics* 8th edn (Wiley)
[26] Singh S and Moons E 2024 Impact of photoinduced phase segregation in mixed-halide perovskite absorbers on their material and device stability *APL Energy* **2** 016112